and equating like coefficients in the two matrices one obtains

$$n = \frac{1 + L'\omega_0^2}{1 + L'C'\omega_0^2}$$

$$C_1 = \frac{(1 + L'\omega_0^2)^2}{L'\omega_0^2(1 + L'C'\omega_0^2)}$$

$$L_1 = \frac{1}{\omega_0^2(1 + L'\omega_0^2)}$$

$$L'' = \frac{1}{1 + L'\omega_0^2}$$

$$C'' = C'\frac{(1 + L'\omega_0^2)^2}{1 + L'C'\omega_0^2}.$$

The latter two equations being those used in the text.

In particular cases it may be found possible to absorb the transformer at some position in the remainder of the network, but it is difficult to formulate meaningful general rules.

*Since submission of this paper it has been drawn to the authors' attention that the low-pass to band-pass transformation where the diode series inductance is considered has been given by Dr. L. I. Smilen in the Polytechnic Institute of Brooklyn, N. Y., Progress Report No. 26, April 1, 1964 through September 30, 1964.*

ACKNOWLEDGMENT

The authors are indebted to Prof. H. J. Carlin of Polytechnic Institute of Brooklyn for a valuable discussion which led to the formulation of the results given in Section VI.

REFERENCES

[1] D. C. Youla and L. I. Smilen, "Optimum negative-resistance amplifiers" *Proc. Symp. on Active Networks and Feedback Systems*, pp. 241–318, April 1960.
[2] R. Aron, "Gain bandwidth relations in negative-resistance amplifiers," *Proc. IRE (Correspondence)*, vol. 49, pp. 355–356, January 1961.
[3] E. S. Kuh and J. D. Patterson, "Design theory of optimum negative-resistance amplifiers," *Proc. IRE*, vol. 49, pp. 1043–1050, June 1961.
[4] W. J. Getsinger, "Prototypes for use in broadbanding amplifiers," *IEEE Trans. on Microwave Theory and Techniques*, vol. MTT-11, pp. 486–497, November 1963.
[5] J. O. Scanlan and J. T. Lim, "A design theory for optimum broadband reflection amplifier," *IEEE Trans. on Microwave Theory and Techniques*, vol. MTT-12, pp. 504–511, September 1964.
[6] L. I. Smilen, "A theory for broadband tunnel diode amplifiers," Polytechnic Institute of Brooklyn, N. Y., Research Rept. PIBMRI-998-62, April 1962.
[7] R. M. Fano, "Theoretical limitations on the broadband matching of arbitrary impedances," *J. Frankin Inst.*, vol. 249, pp. 57–83 and pp. 139–154, January–February 1950.
[8] J. Hamasaki, "A low-noise and wide-band Esaki diode amplifier with a comparatively high negative conductance diode at 1.3 Gc/s," *IEEE Trans. on Microwave Theory and Techniques*, vol. MTT-13, pp. 213–223, March 1965.
[9] L. Weinberg, *Network Analysis and Synthesis*. New York: McGraw-Hill, 1962.

# Locking of Magnetrons by an Injected RF Signal

H. L. THAL, MEMBER, IEEE, AND R. G. LOCK

***Abstract*—An equivalent circuit is given which quantitatively predicts the performance of magnetron oscillators when they are frequency locked by an injected RF signal. A method is presented for the reciprocal coupling of magnetrons to a traveling wave without reflection. The theory is supported by experimental results which include:**

1) **a single-tube locked oscillator with nonreciprocal (circulator) coupling,**
2) **a three-tube locked oscillator array with reciprocal coupling,**
3) **a two-tube oscillator with reciprocal coupling.**

**The feasibility of various locked oscillator and self-oscillating arrays, including the effect of mismatched loads, is discussed.**

Manuscript received April 6, 1965; revised July 23, 1965. The work described was funded by the U. S. Army Electronics Labs., Fort Monmouth, N. J., under Contract DA 36-039 AMC-03409(E).

The authors are with Tube Dept., General Electric Co., Schenectady, N. Y.

## INTRODUCTION

THE ABILITY to lock the frequency of magnetron oscillators allows the application of these high-efficiency devices to systems such as pulse compression or frequency diversity radars which require electronic frequency control or radars which require pulse-to-pulse phase coherence. Furthermore, this ability allows the formation of an array of magnetrons having a coherent output power greater than a single tube. Such an array may consist of separate tubes connected by external circuitry or an extended interaction space within a single vacuum envelope.

The general concept of injection locking an oscillator has been studied by a number of investigators. Adler [1], for example, has made a general analysis of the

steady-state and transient behavior of a single, locked oscillator. David [2], [3] and Donal [4] have considered the specific problem of magnetron locking. Cuccia [5], [6] has reported results on special magnetrons having control grids near the cathode, and Kline [7] has given data on the locking of magnetrons by injecting a signal through a circulator.

The present work [8] has been directed towards relating the gain-bandwidth performance of locked-magnetron arrays to the parameters of the prototype tubes and establishing limits on this performance. Both circulator and reciprocal coupling schemes have been considered. The experimental results have indicated that the equivalent circuit model used is capable of quantitatively predicting the locked performance. The equivalent circuit parameters must be determined experimentally (from a Rieke diagram [9] or locking data) or analytically (from a suitable model of the magnetron interaction). Once they have been obtained, they allow the design to be optimized and the gain-bandwidth limits to be established analytically.

## Locking Theory

Frequency locking of a magnetron is related to the frequency pulling of a magnetron oscillator due to a mismatched load. In frequency locking, a drive signal is supplied by an external source, whereas, in pulling a portion of the magnetron, output is reflected back at the tube. The steady-state operation of a locked magnetron can, in fact, be quantitatively determined from the magnetron Rieke diagram which gives the frequency and power output as a function of the complex load impedance. However, the use of an equivalent circuit model to represent the magnetron allows for an analytical rather than graphical solution to the problem.

Figure 1 shows an equivalent circuit for the magnetron plus circuit elements representing two external coupling cavities and a matched driver. The magnetron equivalent is subdivided into two parts: 1) a parallel resonant circuit representing the cold anode resonator, and 2) a second resonant circuit plus a current generator representing the beam. The current generator has a fixed amplitude $I_m$, but its phase $\theta$ is a variable which must always equal the phase of the total voltage across it. Furthermore, a valid solution exists only when the magnitude of the total voltage across the current generator exceeds a specified minimum value $V_{\min}$.

In this manner, the model simulates the automatic phasing of the electron spokes relative to the voltages on vane tips, and also the abrupt cessation of oscillation that occurs when a magnetron is loaded too heavily. The equivalent beam conductance $G_B$ simulates the output power saturation observed in magnetrons. The equivalent tuned circuit $B_B$ accounts for the frequency sensitivity of the beam and the experimental fact that the "hot" and "cold" frequencies of a magnetron are different (i.e., the current induced into the anode is not exactly in phase with the voltage). A Rieke diagram calculated with equivalent circuit values obtained from a locking experiment is shown in Fig. 2.

In using the model to analyze the locking performance, the approach is to assume the magnetron is locked (i.e., the magnetron is operating at the drive frequency) and then to determine whether such a solution exists (i.e., whether there is any value of $\theta$ that yields a beam voltage in-phase with the generator current and greater than the minimum value). Although Fig. 1 specifically illustrates a third-order output circuit, the analysis may be kept general by representing the entire network between the generators by an impedance matrix. Thus,

$$V_1 = I_1 Z_{11} + I_2 Z_{12}$$
$$V_2 = I_1 Z_{12} + I_2 Z_{22}. \tag{1}$$

Since $V_1$ must have the same phase as the magnetron generator, it may be represented by an amplitude $V_m$ at an angle $\theta$. Also $I_1$ and $I_2$ must equal the magnetron and drive currents respectively. Thus,

$$V_m e^{j\theta} = I_m e^{j\theta}[R_{11} + jX_{11}] + I_d[R_{12} + jX_{12}] \tag{2}$$

where all of the variables are real, and the unknowns are $V_m$ and $\theta$. Multiplying both sides by $e^{-j\theta}$, taking the

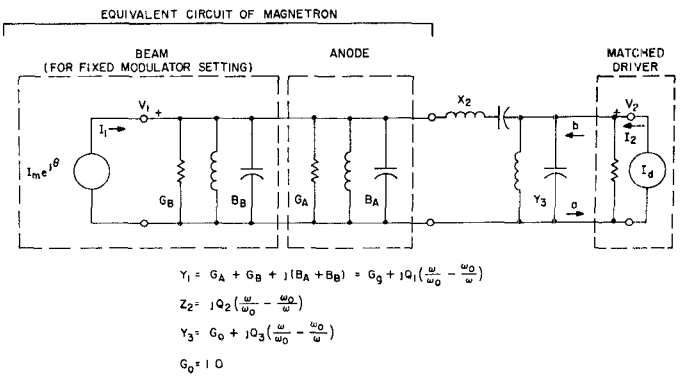


Fig. 1. An equivalent circuit for the magnetron plus circuit elements representing two external coupling cavities and a matched driver.

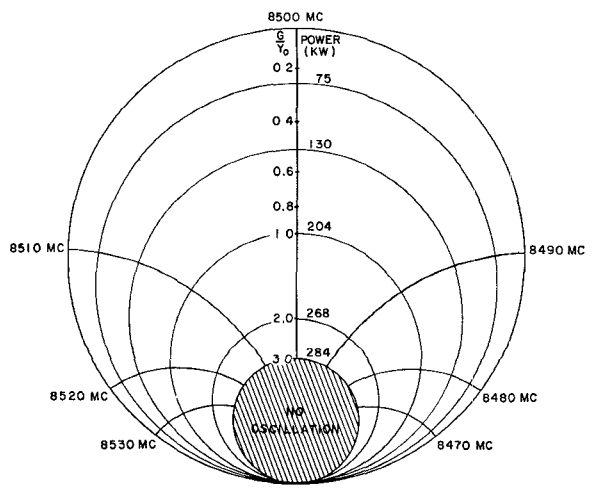


Fig. 2. A Rieke diagram calculated from the equivalent circuit model using typical values for the parameters.

imaginary parts, and solving for $\theta$ yields

$$\theta = \sin^{-1}\left[\frac{I_m X_{11}}{I_d\sqrt{R_{12}^2 + X_{12}^2}}\right] + \tan^{-1}\left[\frac{X_{12}}{R_{12}}\right]. \quad (3)$$

Solving for $V_m$ yields

$$V_m = I_m R_{11} \pm \sqrt{I_d^2(R_{12}^2 + X_{12}^2) - I_m^2 X_{11}^2}. \quad (4)$$

A solution exists if 1) $V_m$ exceeds $V_{\min}$ (lower values of $V_m$ correspond to the nonoscillating region of the Rieke diagram), and 2) the magnitude of the arc sine argument does not exceed unity. Note that the latter quantity is the ratio of the reactive voltage produced by the magnetron generator to the total voltage produced by the driver at the magnetron terminals. Thus, no solution exists if the voltage due to the driver cannot cancel the reactive beam voltage. The first or fourth quadrant arc sine is used since it always results in the larger $V_m$ (i.e., a higher effective impedance) and is therefore assumed to be the stable solution.

Once the angle $\theta$ has been determined, $V_2$ can be calculated directly. If a matched driver is assumed, and the transmission-line impedance is normalized to one ohm, the output and input waves $a$ and $b$ of Fig. 1 are given by

$$a = V_2 - \tfrac{1}{2}I_d \quad (5)$$

$$b = \tfrac{1}{2}I_d. \quad (6)$$

Thus, the relationship between the input and output powers can be calculated directly if the impedance matrix (including the tube elements and driver impedance) is known.

A circuit of the form shown in Fig. 1 is, of course, not useful since the output power is dissipated in the driver. The most direct method of obtaining a practical device is to insert a circulator [7] which allows the input and output waves to be coupled into physically separate transmission lines, as shown in Fig. 3. Thus, the equations derived for a matched driver apply to the circulator coupled magnetron.

In some circumstances it may be impractical or undesirable to use a circulator for coupling. In these cases a reciprocal three-port junction can be substituted [10]. Consider the tee junction shown in Fig. 4. The scattering matrix of this junction is

$$S = \begin{pmatrix} -\frac{K}{K+1} & \frac{1}{\sqrt{K+1}} & \frac{\sqrt{K}}{K+1} \\ \frac{1}{\sqrt{K+1}} & 0 & \sqrt{\frac{K}{K+1}} \\ \frac{\sqrt{K}}{K+1} & \sqrt{\frac{K}{K+1}} & -\frac{1}{K+1} \end{pmatrix}. \quad (7)$$

The transformers have been adjusted to provide a match at port 2 (with ports 1 and 3 matched), so that the magnetron is effectively driven by a matched generator. If the input to the junction is $a_1$, the effective drive $b_2$ flowing towards the magnetron is

$$b_2 = a_1 S_{12} = a_1\left[\frac{1}{\sqrt{K+1}}\right]. \quad (8)$$

Assume that the reference plane and operating point of the magnetron are adjusted at a particular frequency to give

$$a_2 = Kb_2 = a_1\left[\frac{K}{\sqrt{K+1}}\right] \quad (9)$$

where $K$ is a real number. The reverse and output waves become

$$b_1 = 0, \qquad b_3 = \sqrt{K}\, a_1. \quad (10)$$

Therefore,

$$K = \frac{b_3 b_3^*}{a_1 a_1^*} = \frac{P_{\text{out}}}{P_{\text{in}}}. \quad (11)$$

Thus, it is possible to obtain "matched" operation with reciprocal coupling if a portion of the drive signal is intentionally reflected to cancel the reverse wave generated by the magnetron. The power gain of such a stage equals $K$, but by considering the waves actually incident on the magnetron as given by (9), it can be seen that the substitution of a circulator (lossless) would increase the power gain to $K^2$. In the form shown (i.e., matched driver and load) perfect cancellation would occur at only one frequency since the phase between $a_2$ and $b_2$ would vary with frequency. However, by starting with a transmission line periodically loaded with parallel-tuned circuits, it is possible to develop a filter theory which demonstrates that essentially perfect can-

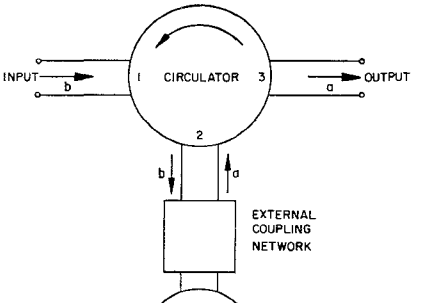


Fig. 3. Diagram of the application of a circulator to separate the output and input waves ($a$ and $b$) of Fig. 1.

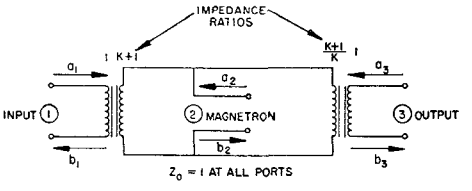


Fig. 4. Diagram of the stepped-impedance tee junction capable of reflectionless coupling with reciprocal elements.

cellation is possible across a finite frequency range if the proper matching sections are used. This filter theory is covered in Appendix I, and experimental evidence will be presented.

The equivalent circuit presented is based on a single-tuned model of the magnetron so that its range of validity is limited by other modes coupled to the output port. If a conventional coupling slot is used, all modes will be coupled. However, if a symmetrical coupling scheme is employed, some modes may not be coupled, and, thus, will not limit the frequency range provided they do not cause spurious oscillations.

The transient response has not been investigated. However, it can be approximated by considering the frequency dependence of the steady-state solution [2], [3]. Such an approximation should be valid provided the envelope of the input wave remains greater than the locking limit and the frequency components are within the locking band.

## Experimental Results

Frequency locking measurements with reciprocal and nonreciprocal coupling have been conducted using standard 6249B magnetrons. No internal modifications of the tubes have been made. The results are intended primarily to demonstrate the concepts involved, but it is assumed that better gain-bandwidth performance could be obtained from a structure specifically designed for locking.

The loaded $Q$ of the magnetron was reduced by an inductive iris in the output waveguide. The addition of this iris formed a second resonant cavity between the iris and the effective reference plane of the magnetron which is located about two wavelengths inside of the tube flange. Fig. 5 illustrates the manner in which the magnetron-iris combination was approximated by a second-order circuit.

Figures 6, 7, and 8 show results obtained with circulator coupling. Both the experimental and computed responses show the entire locking bandwidth (except as noted). The values of $Q_1$ and $Q_2$ were calculated using cold test results plus the equations of Fig. 5. The values of beam current, conductance, and minimum voltage were evaluated from the hot test results.

The curves of Fig. 6 and the top three curves of Fig. 7 were computed with the same equivalent circuit values representing the magnetron. They show the effect of varying $Q_2$ by changing the separation between the iris and the magnetron, and also the effect of varying the drive power. The lower curves of Fig. 7 were obtained with the same physical circuit as the upper curves, but a reduced modulator setting, and, therefore, different equivalent circuit values, were used for the magnetron.

Experiments also have been performed on one-, two-, and three-tube arrays utilizing reciprocal tee junctions of the form shown in Fig. 9. It has been convenient to use series junctions instead of the shunt type shown schematically in Fig. 4. By shifting the reference plane of the magnetron by a quarter wavelength, it is possible to obtain a series-tuned equivalent. In this manner, a filter which is the dual of that described in Appendix I can be developed.

Figure 10 shows the experimental and computed results for a single stage with one input and one output matching section. These results indicate that low reflected power at the input port (i.e., a "hot" match) can be maintained across a frequency band in accordance with the theory. The physical circuit consisted of the magnetron connected to the tee junction with 3.8 VSWR irises in the input and output waveguides five and one-half wavelengths from the center of the tee. For calculations, the irises and lengths of waveguide were replaced by equivalent tuned circuits, in the manner shown in Fig. 5.

Figure 11 gives the results of a two-tube array. In the absence of drive, an oscillating mode was observed at 8555 Mc/s with forward and reverse powers at 568 and 36 kW. The model predicted a mode at 8556 Mc/s with outputs of 498 and 66 kW plus a similar mode at 8518 Mc/s. In order to have both stages operating with the same effective load impedance, it was necessary to couple the second stage more heavily in order to compensate for its larger input power. In this manner, both tubes operated at the same modulator setting, and contributed equally to the total output power. Since the first stage had lighter coupling, it had the smaller bandwidth of the two stages, and was the one that primarily determined the bandwidth of the array. Physically, the circuit consisted of two tee junctions designed to give zero reflected power for their respective stages. An inductive iris was located between each magnetron and its tee junction. The iris VSWR's for the first

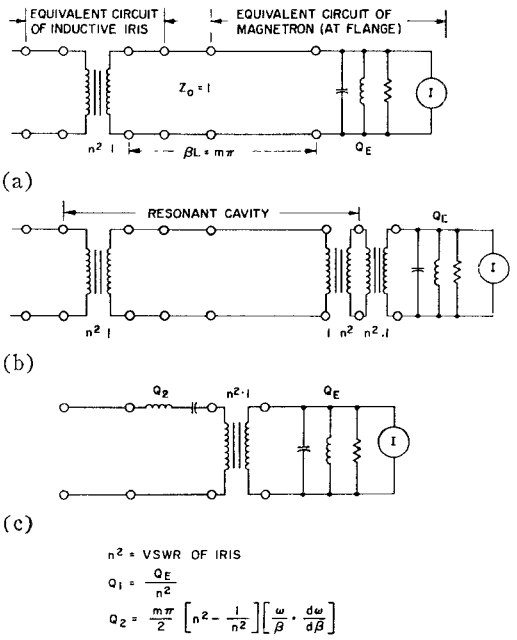


Fig. 5. Illustration of the manner in which the combination of a magnetron and an external inductive iris was approximated by a second-order circuit.

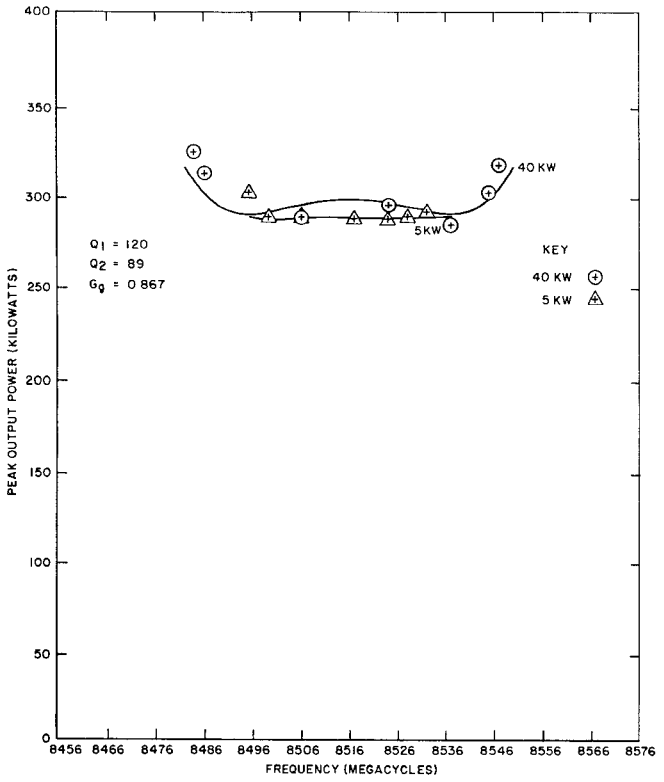


Fig. 6. Computed (curve) and measured (points) output power of a circulator-coupled magnetron for varying drive frequency and drive power.

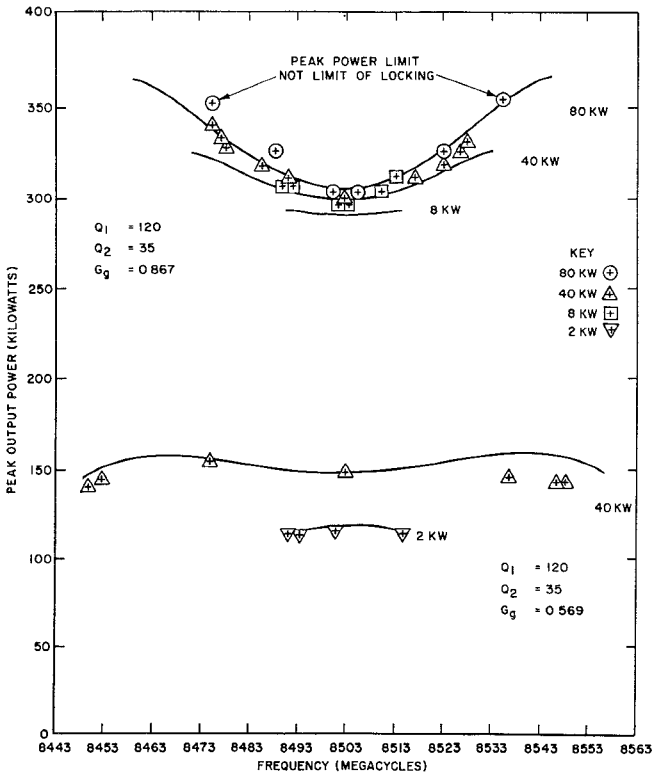


Fig. 7. Computed and measured output power for a circulator-coupled magnetron for varying drive frequency, drive power, and modulator setting.

and second stages were 3.8 and 7.6, respectively. (These values took into account the variation in the external $Q$'s of the two magnetrons.)

An additional stage was added at the input end to form a three-tube array. The experimental configuration is pictured in Fig. 12, and the results are given in Fig. 13. This extra stage was loaded in the same manner (i.e., the same tee and iris) as the first stage of the two-tube array, but it was operated at a lower modulator setting so that it could be locked with a smaller drive signal.

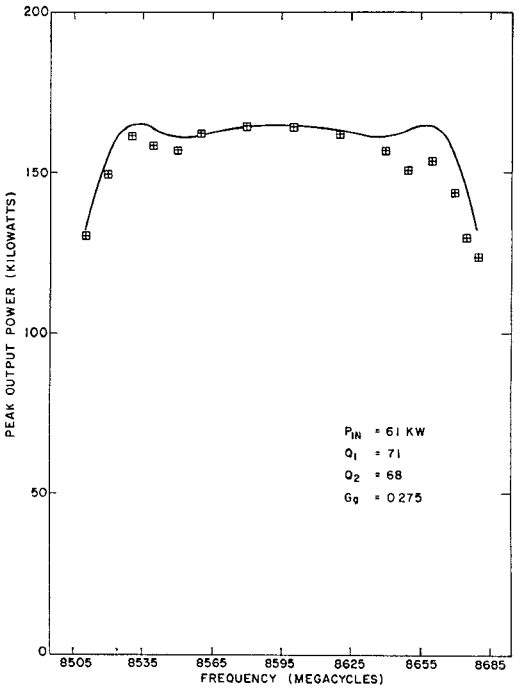


Fig. 8. Computed and measured output power for a circulator-coupled magnetron demonstrating agreement over a 165-Mc/s frequency range.

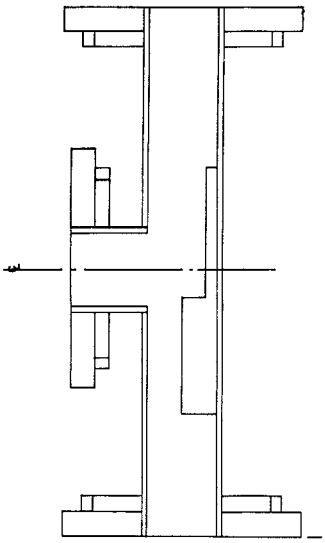

Fig. 9. Physical embodiment of the series tee junction corresponding to the parallel junction of Fig. 4.

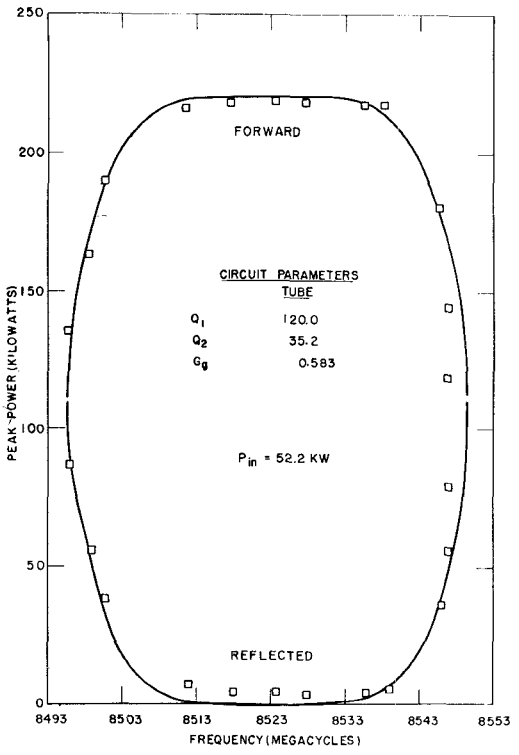


Fig. 10. Computed (curve) and measured (points) forward and reverse power output from a single reciprocally coupled magnetron.

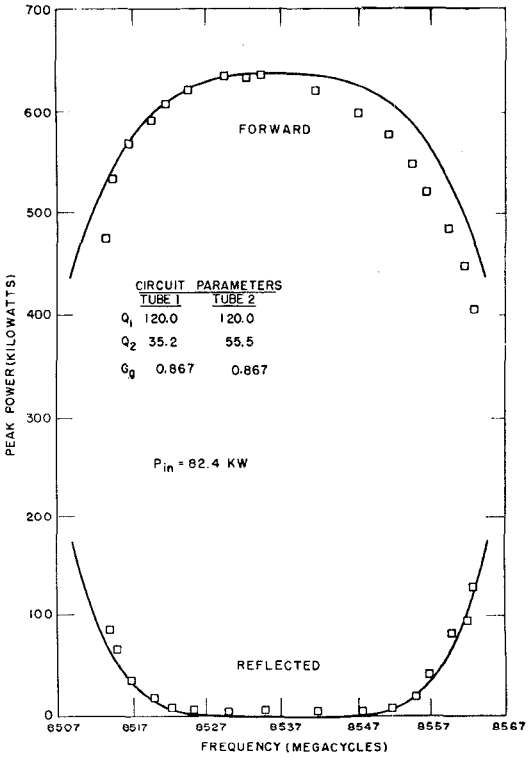


Fig. 11. Computed and measured forward and reverse power output from a two-tube array of reciprocally-coupled magnetrons.

Thus, the gain of the array was increased by approximately 6 dB with a relatively small reduction in bandwidth. All three magnetrons were run from the same low impedance modulator. The individual operating points were set by using a 600-ohm resistor in series with the first magnetron, and resistances of approximately 250 ohms for the other two tubes.

The second and third stages were also tested as a two-tube oscillator. For this experiment, the second magnetron was coupled directly (without iris or tee) to the input of the third stage. The third stage utilized the same iris and tee as in the three-tube array (even though these were not quite optimum for the oscillator application). A peak output power of 575 kW at 8535 Mc/s was obtained. Both tubes had the same average current, and, therefore, should have contributed approximately equally to the output power.

Fig. 12. Experimental three-tube array of reciprocally-coupled magnetrons.

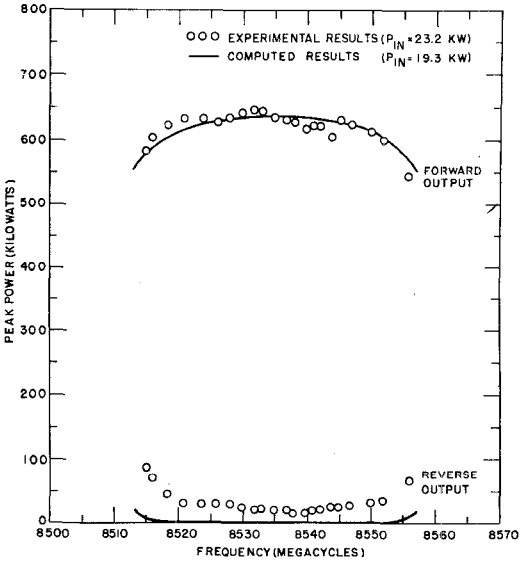


Fig. 13. Computed and measured forward- and reverse-power output from a three-tube array of reciprocally-coupled magnetrons.

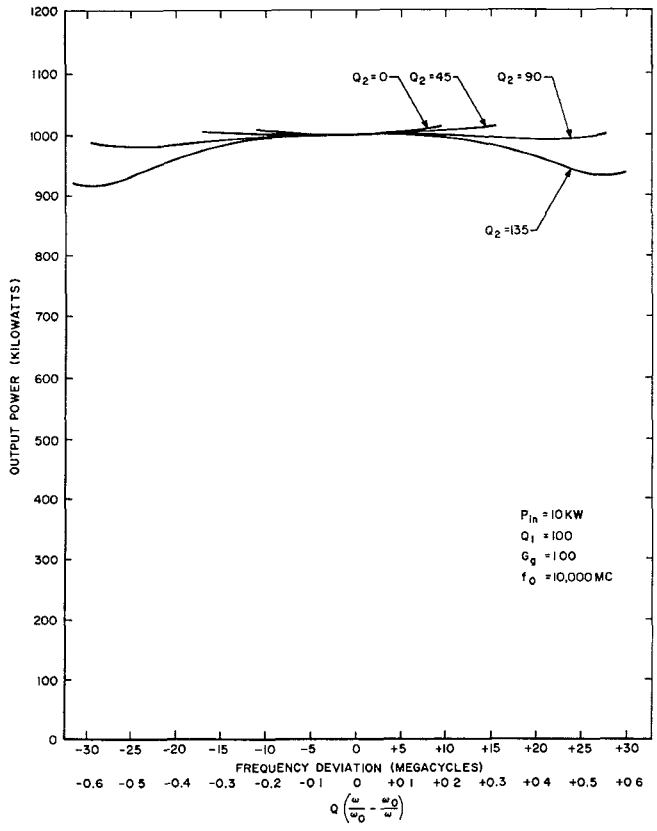


Fig. 14. Computed performance of a circulator-coupled magnetron demonstrating the improvement possible with second-order circuits compared with a simple resonant cavity ($Q_2=0$).

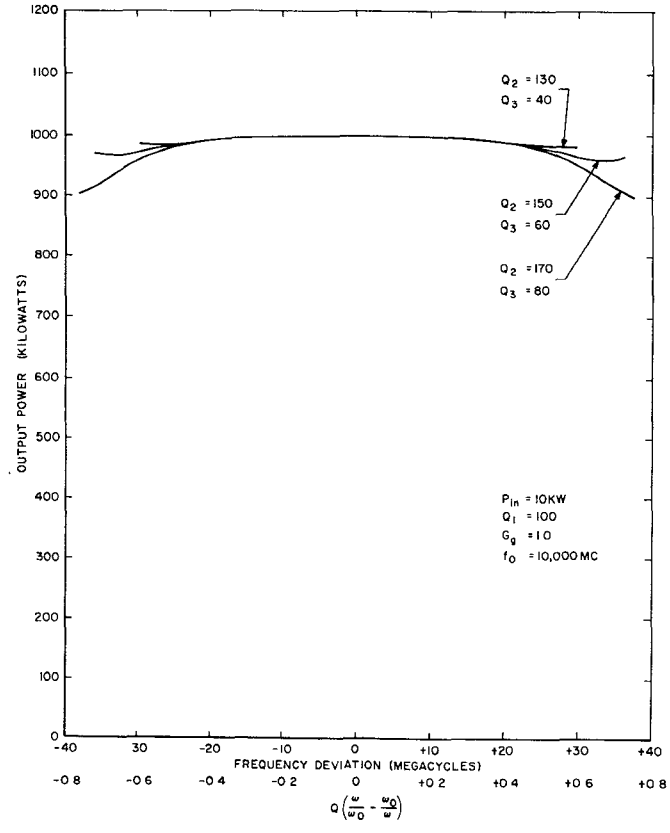


Fig. 15. Computed performance of a circulator-coupled magnetron with a third-order circuit.

## Computed Performance

### *Circulator Coupling*

The equivalent circuit model has provided a convenient means for investigating a number of locking configurations, in addition to those experimentally verified. First, consider the use of multiply-tuned output circuits in a magnetron with circulator coupling. Figure 14 illustrates the bandwidth improvement that is possible with a second-order circuit compared with a simple resonant cavity ($Q_2=0$). (All of these responses are based on the equivalent circuit of Fig. 1 and have a beam voltage of 1556 at midband.) Figure 15 shows the further improvement that is possible with third-order circuits.

As a more specific example, assume a tube having $Q_1=100$, $I_m=2828$, $G_g=1.0$, $V_{\min}=1556$, and a minimum power gain of 20 dB. From the equation of Appendix II and the curve of Fig. 15, the respective bandwidths for 1) an optimum single-tuned circuit; 2) a third-order circuit with $Q$'s of 100, 150, and 60; and 3) an "ideal" network (see Appendix II) would be 17, 72, and 158 Mc/s. Thus, a third-order circuit can have more than four times the single-tuned bandwidth and almost one half that of an ideal network.

### *Mismatched Array*

Although it is possible to design high gain arrays using the filter approach described in Appendix I, computed results have disclosed that such arrays are sensitive to load mismatches. The reason for this effect is demonstrated in Appendix III. At midband, where the phase shift per section is 90°, a reverse wave may be either amplified or attenuated, depending on its phase. Further, the phase shift per stage of this reverse wave is such that the effect is cumulative for an array of stages. If the array is divided into two sections with 45° phase shift between, a reflected wave, which is amplified in one section, will be attenuated in the other, so that the net amplification may be made approximately unity. However, the addition of the 45° of phase shift upsets the matched load performance at all frequencies except midband, and thereby reduces the useful bandwidth appreciably.

As an example of this mismatched behavior, Fig. 16 shows the reflection coefficient locus at the input as a 1.1-VSWR load as the output is moved through all phases. This array has six stages and 10-dB gain. Changing the phase shift between the second and third stages to 45° yields the approximately circular contour shown.

In order to determine whether the "impedance-stepped" design was unusually susceptible to load mismatches, two five-tube arrays—one with impedance stepped tee junctions and one with symmetrical tees—were designed and computed. Although the uniform

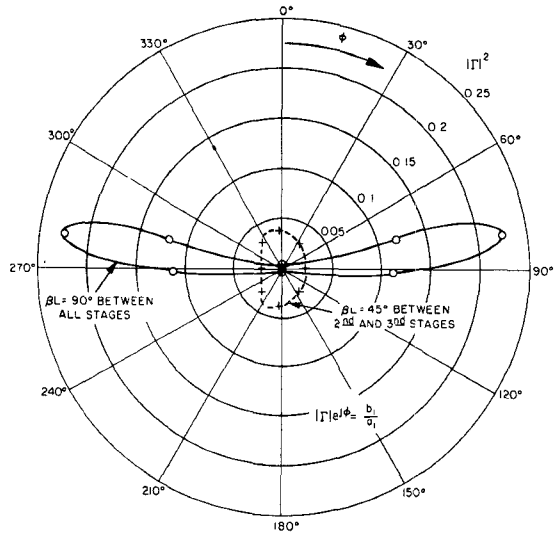


Fig. 16. Computed input power reflection coefficient at resonance for a six-tube, 10-dB gain array as a 1.1-VSWR load is moved through all phases.

array was adjusted to give comparable matched load performance (i.e., negligible reverse output) at midband, its matched load bandwidth was less, and it also exhibited a reverse gain equal to the forward gain for certain phases.

*Composite Array*

A composite array consisting of a circulator-coupled gain stage followed by low-gain, stepped-impedance power stages offers good gain and stability, plus high output power. The use of a four-port circulator with a dummy load allows a good gain-bandwidth performance for the first stage, with isolation from the effects of load mismatches. The use of tee junctions in the low-gain power stages avoids the use of additional circulators with their losses and power handling limitations, but does not appreciably affect the overall bandwidth and stability. (If the tee junctions are not within the vacuum envelope, they may limit the peak power.)

As an example, consider such a composite array of four tubes, each of which has a matched load output of 200 kW and can be represented by $I_m = 1265$; $G_g = 1.0$; $Q = 50$; $V_{\min} = 450$. The computed output power and gain are 793 kW and 21 dB over a locking range of 3.4 per cent. Only the first stage employs a circulator, and it has to handle a forward power of 197 kW and maximum reverse powers of 45 kW and 130 kW for 1.25 and 1.5 VSWR-loads.

*Oscillator Array*

If an oscillator with more output than a single magnetron is required, an array can be designed, consisting of a first-stage oscillator followed by power stages. Nonreciprocal devices are not necessary as long as the total gain of the power stages is relatively low. A three-tube array has been designed, using for each stage the equivalent circuit that yields the Rieke diagram of Fig. 2.

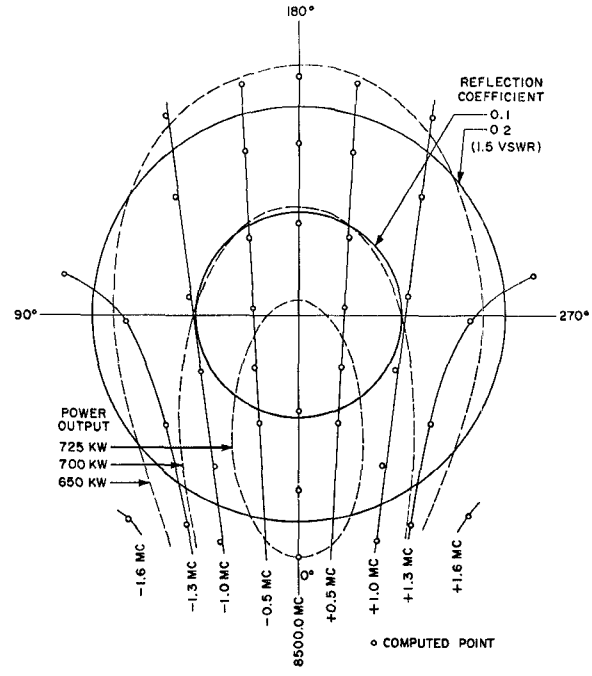


Fig. 17. Computed Rieke diagram demonstrating the mismatched load performance of a three-tube oscillator array.

A stabilizing cavity was used with the first stage to increase its effective $Q$ to 2100. The tee junctions and coupling transformers of the other stages were adjusted for "reflectionless" operation with the same net power output as the oscillator stage. The separation between stages was 90°.

The Rieke diagram of the array is shown in Fig. 17. The matched load output is 727 kW. For a 1.5-VSWR load, the relative output power varies between 1.01 and 0.85. A single prototype tube, adjusted for the same matched load output as each stage of the array, would have a relative power variation of 1.12 to 0.82 for a 1.5-VSWR load.

## Conclusions

1) An equivalent circuit has been developed which, with a minimum number of experimentally determined constants, quantitatively predicts the performance of magnetrons as locked oscillators. This model can be applied to a magnetron array which can be solved by utilizing an iterative solution and a computer.

2) Multiple-tuned circuits for circulator-coupled magnetrons, such as those demonstrated, provide frequency locked operation with gain-bandwidth products approaching the theoretical limit.

3) The stepped-impedance tee-junction filter design provides reflectionless reciprocal coupling to a traveling wave over a band of frequencies.

4) The usable gain of reciprocally coupled devices is limited by sensitivity to load mismatch. However, feasibility has been demonstrated for locked oscillator and self-oscillating arrays employing combinations of nonreciprocal and reciprocal coupling.

## Appendix I
## Filter Theory

By considering a single tube in the circuit of Fig. 4, it was shown that it is possible to obtain "matched" operation with reciprocal coupling at a single frequency. A match can be maintained over a band of frequencies for an infinite filter formed by periodically loading a waveguide with tubes. The $N$th section of such a filter is shown in Fig. 18. The waves traveling forward and backward between the $N-1$ and $N$th sections are $a_N$ and $b_N$, so that the voltage and current half way along the line between stages are

$$V_N = a_N e^{j(\beta L/2)} + b_N e^{-j(\beta L/2)}$$
$$I_N = a_N e^{j(\beta L/2)} - b_N e^{-j(\beta L/2)}. \tag{12}$$

Consider first the passive filter ($I_m = G_g = 0$, $K = 1$). A match occurs when

$$\frac{I_N}{V_N} = \frac{I_{N+1}}{V_{N+1}} = Y,$$

the characteristic admittance of the filter at this plane. When $\beta L = \pi/2$

$$Y = \sqrt{\frac{T^2 + B}{T^2 - B}} \tag{13}$$

where $T^2$ is the impedance ratio of the coupling transformer between the tube and the tee junction, and $B$ is the susceptance of the equivalent magnetron resonator. The characteristic admittance $Y$ is real for the pass-band frequencies $\omega$ between

$$\omega_{1,2} = \omega_0 \left[ \sqrt{1 + \left(\frac{T^2}{2Q_1}\right)^2} \pm \frac{T^2}{2Q_1} \right]. \tag{14}$$

The same matched condition is maintained for the active filter if

$$\frac{I_m}{V_m} = G_g + \frac{K-1}{K+1}\sqrt{1+B^2}. \tag{15}$$

Thus, a hot match can be maintained for the entire band pass of the filter if the forward waves satisfy

$$|a_N| = \frac{1}{2} I_m \frac{\sqrt{K+1}}{K-1} \frac{\sqrt{T^2+B} + \sqrt{T^2-B}}{\sqrt{T^4 - B^2} + \frac{K+1}{K-1} G_g} \tag{16}$$

and

$$|a_{N+1}| = \sqrt{K}\,|a_N|.$$

The reflected waves are

$$\left|\frac{b_N}{a_N}\right| = \left|\frac{b_{N+1}}{a_{N+1}}\right| = \frac{\sqrt{T^2+B} - \sqrt{T^2-B}}{\sqrt{T^2+B} + \sqrt{T^2-B}} \tag{17}$$

so that, while the filter is matched over the pass band, the waveguide is matched only at resonance.

To maintain a perfect match, the filter would not only have to be infinite, but also (13) and (16) would have to be satisfied for each successive stage, which severely restricts the choice of parameters. That is,

$$\frac{B}{T^2} \quad \text{and} \quad \frac{K+1}{K-1}\frac{G_g}{T^2}$$

must be the same for each stage, and

$$\frac{I_{m(N+1)}}{I_{m(N)}} = \sqrt{\frac{K_N(K_N+1)}{K_{N+1}+1}}\,\frac{K_{N+1}-1}{K_N - 1}. \tag{18}$$

However, the perfect match can be approximated for practical arrays allowing more latitude in design. The following method provides a match at three frequencies. Figure 19(a) illustrates the other plane of symmetry for which the passive filter has a real characteristic admittance

$$Y' = \frac{1}{2}\sqrt{1 - \left(\frac{B}{T^2}\right)^2}. \tag{19}$$

Figure 19(b) shows a matching stage between two semi-infinite filters of characteristic admittances

$$Y_A' = \frac{1}{2}\sqrt{1 - \left(\frac{B}{T_A^2}\right)^2}$$

and

$$Y_B' = \frac{1}{2}\sqrt{1 - \left(\frac{B}{T_B^2}\right)^2}. \tag{20}$$

A match occurs at resonance and two other symmetrically located frequencies satisfying

$$\left(\frac{B}{T_1^2}\right)^2 = \frac{\sqrt{1 - \left(\frac{B}{T_A^2}\right)^2}}{\sqrt{1 - \left(\frac{B}{T_B^2}\right)^2}} - 1 + \left(\frac{B}{T_A^2}\right)^2$$

$$\left(\frac{B}{T_2^2}\right)^2 = \frac{\sqrt{1 - \left(\frac{B}{T_B^2}\right)^2}}{\sqrt{1 - \left(\frac{B}{T_A^2}\right)^2}} - 1 + \left(\frac{B}{T_B^2}\right)^2. \tag{21}$$

Figure 19(c) indicates a return to the normal reference planes of Fig. 18. Note that with these reference planes, two stages (only one of which is shown) are involved in matching rather than one. Figure 19(d) shows an active stage substituted for the passive stage of Fig. 19(c). The parameters $I_m$, $G_g$, $K_3$, and $T_3$ are determined from the design of the array providing a match at resonance. The match is approximated at the same two frequencies off resonance by setting

$$D_3 = \frac{T_3^2}{K_3+1}\left(\frac{1}{T_A^2} + \frac{K_3}{T_1^2}\right)$$

$$D_4 = \frac{T_4^2}{K_4+1}\left(\frac{1}{T_2^2} + \frac{K_4}{T_B^2}\right). \tag{22}$$

A slight mismatch remains because condition (16) is not exactly satisfied. In practical cases, this effect is small.

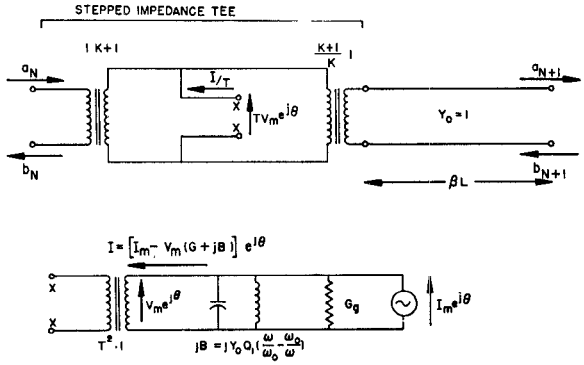


Fig. 18. Circuit diagram of the $N$th section of an infinite filter formed by periodically loading a waveguide with tubes.

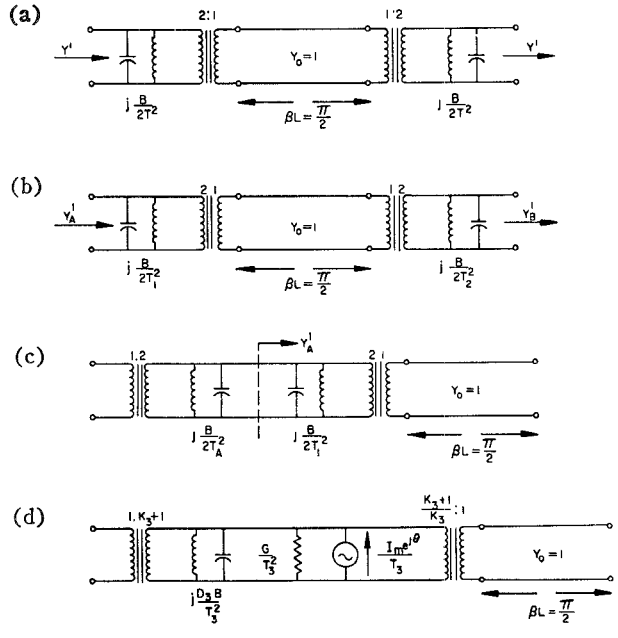


Fig. 19. Circuit diagrams employed to demonstrate the design of filter matching sections.

Since $Q$ is taken to represent the minimum value associated with the chosen tube parameters, the factors $D$ must be equal or greater than one. This represents a small additional "dummy" reactive loading. Matching transitions to the input and output waveguides of the array are obtained by letting $T_A$ or $T_B$ go to infinity. Since the reflected wave is rereflected by such an input transition, the power to be supplied by the driver is essentially $\frac{1}{2}(|a_N|^2-|b_N|^2)$, which is plotted in Fig. 20. For typical values of

$$\frac{K+1}{K-1}\frac{G_g}{T^2},$$

a constant drive power is a reasonable approximation over most of the band. The practical application of this filter theory is demonstrated by the computed performance of a six-tube 10-dB gain array shown in Fig. 21.

## Appendix II

## Gain-Bandwidth Limitations

Based on the magnetron model of Fig. 1, it is possible to compute the maximum locking range for a particular

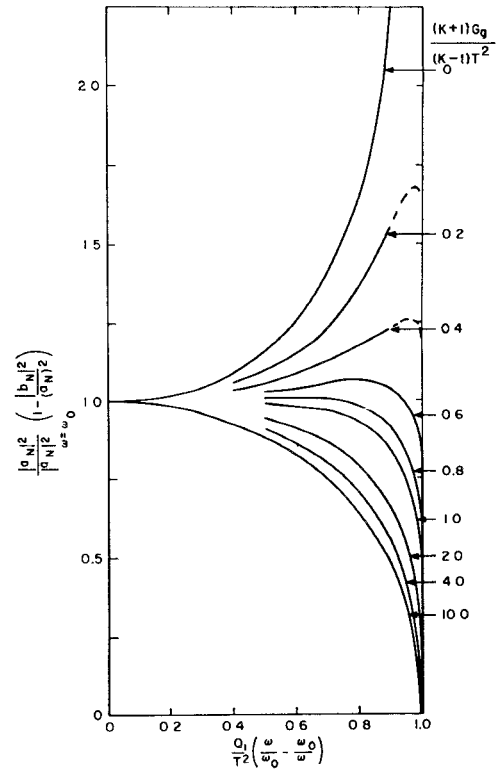


Fig. 20. Calculated drive power required to maintain a perfect match over the pass band of the prototype filter with perfect input and output matching.

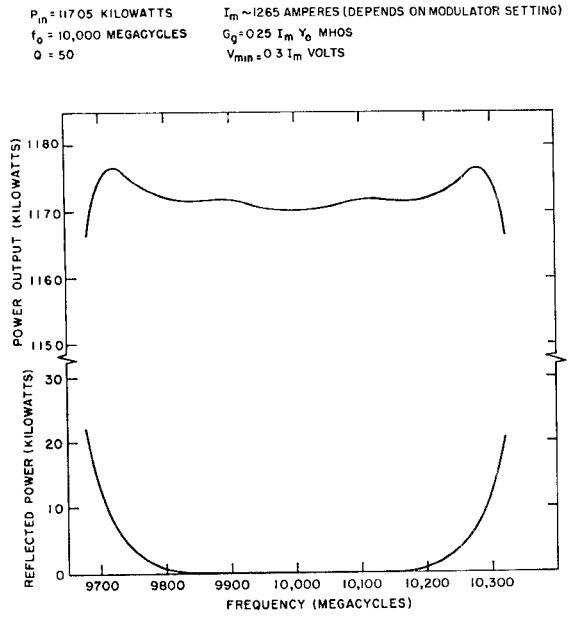


Fig. 21. Computed power output of a six-tube, 10-dB gain array of reciprocally-coupled magnetrons demonstrating matched-load performance of arrays designed according to the filter theory.

single tube with nonreciprocal coupling at a particular modulator setting and gain. If the value of $Q_1$ is adjusted to alter the bandwidth, the values of $I_m$, $G_g$, and $V_{min}$ must also be adjusted, since any variation of $Q_1$ corresponds essentially to placing a transformer between the tube and the external circuitry. That is, the equivalent circuit parameters for a given tube may be transformed as

$$Q_1' = n^2 Q_1 \qquad I_m' = nI_m$$

$$G_g' = n^2 G_g \qquad V_{\min}' = \frac{1}{n} V_{\min}.$$

For the special case of a single-tuned circuit, the maximum bandwidth is obtained when the beam voltage drops to $V_{\min}$ at the same frequencies at which the arc sine of (3) goes to $\pm 90°$. If the equivalent circuit of a tube for a particular output coupling is known, this optimum condition may be obtained by transforming the equivalent circuit by

$$n^2 = \left(\frac{K-1}{K+1}\right)\left(\frac{I_m}{V_{\min}} - G_g\right)^{-1} \tag{23}$$

where $K$ is the desired band-edge power gain. The resulting bandwidth is

$$\frac{\Delta f}{f_0} = \frac{2}{Q_1}\frac{\sqrt{K}}{[K-1]}\left(\frac{I_m}{V_{\min}} - G_g\right). \tag{24}$$

Since the tube equivalent circuit includes a shunt capacitance, it is possible to apply Bode's integral theorem [11] to determine a theoretical limit on the gain-bandwidth. This limit would be achieved if the tube were coupled by an "ideal" network, presenting to the beam at every frequency in the desired band, a constant real impedance of the maximum value allowed by Bode's theorem. In this case, the gain and bandwidth would be related by

$$\frac{\Delta f}{f_0} = \frac{\pi}{2Q_1}\sqrt{\frac{K+1}{K-1}}\left(\frac{I_m}{V_{\min}} - G_g\right). \tag{25}$$

## Appendix III

## Mismatched Loads

Consider a general section of an array as shown in Fig. 18 when $\beta L = 90°$ and $\omega = \omega_0$. In this condition, $b_N$ and $b_{N+1}$ are zero for matched load operation; but in order to study the effects of a mismatch, assume that a small $b_{N+1}$ exists. This wave travels back towards the tee junction, and a portion of it is coupled into the tube arm, thereby modifying the net drive on the tube. It will be shown that for certain phases of this reverse wave, it is amplified, while for other phases, attenuation occurs.

The scattering coefficients of the tee junction and the relationship between the waves for matched operation (not including 90° line) are given in (7) through (10). (The effect of the line can be included by multiplying $S_{13}$ and $S_{23}$ by $-j$, $S_{33}$ by $-1$, and the right side of equation 10 by $-j$.) First, let the forward and reverse waves at the output be related by

$$b_{N+1} = \pm jMa_{N+1} = \pm jM[-j\sqrt{K}\, a_N] \tag{26}$$

where $M$ and $K$ are real. Then, the net wave incident on the magnetron becomes

$$b_2 = a_N\left[\frac{1}{\sqrt{K+1}} \mp jM\frac{K}{\sqrt{K+1}}\right]. \tag{27}$$

For small values of $M$, the magnitude of $b_2$ remains essentially unchanged, but its phase is rotated. Thus, the wave leaving the magnetron $a_2$ is similarly rotated, and equals $Kb_2$. Adding the contributions of $a_N$, $b_{N+1}$, and $a_2$ yields for the reverse wave at the input

$$b_N = \mp jMKa_N = -j\sqrt{K}\, b_{N+1}. \tag{28}$$

Thus, a small reverse wave in this phase is amplified in exactly the same manner as a forward wave, and if 90° sections are cascaded, the gain is cumulative.

Next, consider a reflected wave with a phase which is different by 90°. Thus,

$$b_{N+1} = \pm Ma_{N+1}$$

$$b_2 = a_N\left[\frac{1}{\sqrt{K+1}} \mp M\frac{K}{\sqrt{K+1}}\right].$$

In this case, the amplitude, rather than the phase of $b_2$, is changed. Since the magnetron is assumed to be at resonance, the phase of the current generator is unchanged. The reverse wave at the input (provided the generator voltage remains above its minimum value) is obtained from the "cold" propagation through the section.

$$b_N = -j\left[\frac{2}{1+\frac{G_g}{T^2}}\right]\left[\frac{\sqrt{K}}{K+1}\right]b_{N+1}.$$

Thus, a small reverse wave in this phase is attenuated, and for an array of 90° sections, the attenuation is cumulative.

## Acknowledgment

Much of the experimental work described was performed by J. L. Mundy.

## References

[1] R. Adler, "A study of locking phenomena in oscillators," *Proc. IRE*, vol. 34, pp. 351–357, June 1946.
[2] E. E. David, Jr., "RF phase control in pulsed magnetrons," *Proc. IRE*, vol. 40, pp. 669–685, June 1952.
[3] E. E. David, Jr., and E. Okress, Ed., *Crossed-Field Microwave Devices*, vol. II, New York: Academic Press, 1961, pp. 375–399.
[4] J. S. Donal, Jr., and L. Marton, Ed., *Advances in Electronics*, vol. 4, New York: Academic Press, 1952, pp. 188–254.
[5] C. L. Cuccia, "Frequency-locked, grid-controlled magnetron," *RCA Rev.*, vol 21, pp. 75–93, March 1960.
[6] C. L. Cuccia and E. Okress, Ed., *Crossed-Field Microwave Devices*, vol. II, New York: Academic Press, 1961, pp. 83–91.
[7] J. Kline, "The magnetron as a negative-resistance amplifier," *IRE Trans. on Electron Devices*, vol. ED-8, pp. 437–442, November 1961.
[8] H. L. Thal and R. G. Lock, "Superpower millimeter wave tube," General Electric Co., Schenectady, N. Y., Final Report of Contract DA 36-039 AMC-03409(E), November 15, 1964.
[9] A. G. Smith and G. B. Collins, Eds., vol. 6, M.I.T. Rad. Lab. Ser., New York: McGraw-Hill, 1948, chap. 19.
[10] H. L. Thal, "Superpower millimeter wave tube," Final Report of Contract DA 36-039 AMC-00031(E), September 15, 1963.
[11] H. W. Bode, *Network Analysis and Feedback Amplifier Design*. Princeton, N. J.: Van Nostrand, 1945, pp. 276–283.